Aerosol and Air Quality Research

ORIGINAL RESEARCH
https://doi.org/10.4209/aaqr.240015

Rapid Built-up of PM_{10} in the Ambient Air of the Leeward Side Resulting from Strong Pressure Gradient Force Associated with Density Current

Wei-Kuo Soong[1], Chung-Hsuang Hung[2*]

[1] Department of Military Meteorology, Air Force Institute of Technology, Kaohsiung 820, Taiwan
[2] Department of Safety Health and Environmental Engineering, National Kaohsiung University of Science and Technology, Kaohsiung 824, Taiwan

ABSTRACT

Meteorological factors can result in air pollution. Some studies have indicated that the leeward side effect's weak flow and subsidence play major roles in inducing high PM_{10} (particulate matter with a diameter of $\leq$ 10 μm) in southern Taiwan during winter due to topographic blocking. However, the results of this research showed that the rapid build-up of high PM_{10} in Kaohsiung city (KHC) during evenings is not completely explained by weak flow and subsidence. In northern Taiwan, topographic blocking on northwesterly enhances a significant pressure gradient force (PGF) induced strong winds. According to the Froude number (above 0.5), the flow in northern Taiwan can pass the terrain, producing subsidence warming in central Taiwan, which is located at the leeward side of the northeastern Central Mountain Range (CMR). In addition, strong winds blew river dusts in the middle of Taiwan under a stable atmosphere and stimulated density current, transporting PM_{10} to southern Taiwan. A large horizontal pressure gradient was still formed in central western Taiwan between the cold flow originating from northern Taiwan and the warm flow by subsidence warming. The strong PGF and the interaction between the flow and the terrain in northern Taiwan should favor the density current. After PM_{10} was transported into KHC efficiently in a short time by the density current, the local effect of weak rear flow and subsidence in KHC enhanced and maintained PM even more than it did in central Taiwan.

Keywords: PM_{10}, Density current, Inversion, Pressure gradient force

Received: January 15, 2024
Revised: June 26, 2024
Accepted: June 28, 2024

* **Corresponding Author:**
jeremyh@nkust.edu.tw

Publisher:
Taiwan Association for Aerosol Research
ISSN: 1680-8584 print
ISSN: 2071-1409 online

1 INTRODUCTION

Due to growing economic activities in Taiwan, air pollution has become a serious issue. Airborne-suspended particulate matter (PM) is an important marker of poor air quality in Taiwan. PM has seasonal and daily variation due to meteorological factors (Alizadeh Choobari *et al.*, 2016; Mobarak Hassan and Alizadeh, 2022; Ali *et al.*, 2015; Xing and Sun, 2022), such as atmospheric planet boundary layer (PBL) and circulation (Alizadeh Choobari *et al.*, 2012; Hsieh *et al.*, 2022; Hsu and Chen, 2019; Soleimanpour *et al.*, 2023; Sun *et al.*, 2019, 2021). High PM occurs frequently between late fall and mid-spring, which is related to the Winter Asia Monsoon (WAM) (Zhang *et al.*, 2017). Northeasterly winds often occur in northeastern Taiwan during winter when the flow is strong enough to pass the Central Mountain Range (CMR) and induce subsidence in Kaohsiung city (KHC), located on the leeward side of Taiwan. However, despite the northeasterly winds not being strong enough to pass CMR, the large-scale environment still has a high pressure enough to induce subsidence over KHC. Such subsidence inversion favors air pollution (Hung and Lo, 2015; Largeron and Staquet, 2016; Olofson *et al.*, 2009; Silva *et al.*, 2007; Sun *et al.*, 2018; Wallace and Kanaroglou, 2009; Xu *et al.*, 2019; Zhang *et al.*, 2009; Zhai *et al.*, 2019). Besides subsidence in the leeward side's effect, the weak rear flow phenomenon occurs as northeasterly winds reach CMR due to terrain blocking. In this study, the effect on the leeward side, including weak rear flow

and subsidence, is called the "leeward side effect". It leads to the accumulation of high PM_{10} (Hung *et al.*, 2018; Hsu and Cheng, 2016; Hsu *et al.*, 2016; Hsu and Cheng, 2019; Wang and Chen, 2008).

In addition, KHC's high PM_{10} may be induced by long-range transporting. Many studies showed that strong flow could transport PM_{10} downstream in the atmosphere even for hundreds or thousands of kilometers (Duce *et al.*, 1980; Lin *et al.*, 2004, 2005, 2007, 2012; Lin, 2001; Prospero *et al.*, 2003; Wuebbles *et al.*, 2007; Wang *et al.*, 2000; Amodio *et al.*, 2011; Wang *et al.*, 2015; Wang *et al.*, 2017). Regarding Zhuoshui River (ZSR) dust in Central Taiwan, when WAM is significant, strong flow not only blow ZSR dust, but also favor transporting the dust from the bare soil formed to the river's downstream under certain drought atmospheric conditions (Kuo *et al.*, 2010, 2014; Lin *et al.*, 2016; Chuang *et al.*, 2016; Kuo *et al.*, 2017; Lin *et al.*, 2018; Weng *et al.*, 2021). The most serious event of ZSR's dust transported southward occurred on November 2, 2009. According to the Ministry of Environment (MOENV) report, the dust of ZSR could even affect as far as southern Taiwan. Lin *et al.* (2018) also analysed the ZSR dust event, and found that the strong WAM prevailed for more than 30 hours, spreading the ZSR dust downstream to western Taiwan. Hence, high PM_{10} owing to dust is common during late winter and spring in East Asia and Taiwan (Duce *et al.*, 1980; Chen and Chen, 1987; Wang and Chen, 2008; Shaw, 1980; Parrington *et al.*, 1983; Lin *et al.*, 2004; Huang *et al.*, 2018).

Both long-range transport and the leeward effect may cause high PM_{10} concentrations in KHC. However, increasing high PM_{10} concentrations in just a few hours requires a quantitative analysis of the correlation between air pollution, meteorological conditions, and KHC's geographic environment. In the past, much literature has investigated the leeward side's effect on air pollution in south-central Taiwan. However, there is almost no literature discussing the long-range transportation of suspended particle effects on the rapid accumulation of PM in southern Taiwan. Crouvi *et al.* (2017) pointed out that density current could rapidly transport dust. Density current—also called gravity current (Ising *et al.*, 2022; Stancanelli *et al.*, 2018) and often found in nature (Hallworth *et al.*, 2001; Birman *et al.*, 2007; Musumeci *et al.*, 2017; Huppert, 1982). A density current is a region of dense fluid that moves into an environment of less dense fluid. Density currents can occur with sea-breeze fronts, cold fronts, drylines, and can also be associated with an outflow from a thunderstorm (Evan *et al.*, 2022; Ising *et al.*, 2022). In some cases, surface cold fronts move at speeds faster than the normal component of the wind because the front has the nature of density current (Smith and Reeder, 1988; Chen and Hui, 1990). One of the common atmospheric phenomena of density flow is cold air damming, which is related to the terrain blocking the cold air (Lagouvardos *et al.*, 1988; Smith and Reeder, 1988). In Taiwan, northeasterly winds in winter or cold air behind or at the front during summer may be blocked by CMR, thus resulting in significant pressure gradient force (PGF), which may trigger the phenomenon of cold air damming (Chen and Hui, 1990; Chen and Kuo, 2006). Whether or not the fast-moving speed of density currents contributed to the rapid increase in PM_{10} concentration in KHC is an issue worth exploring. Therefore, this paper aims to investigate the conditions for the formation of density current and its effect on the build-up of PM_{10} in southern Taiwan. In particular, it probes into the influence of central Taiwan's river dust on PM_{10} in KHC through density current and leeward side effects by conducting a case study and numerical modelling. Section 2 describes the methodology and the Weather Research & Forecasting Model (WRF). Section 3 discusses the effects of density current behaviour associated with leeward side effects on PM_{10} in KHC, and Section 4 presents the conclusions.

2 MATERIALS AND METHODS

2.1 Research Area and Data

On January 26 and 27, 2018, the synoptic flow was northeasterly around Taiwan. The PM_{10} on the 26th was twofold stronger than on the 27th. The flow speed on the 26th was stronger than on the 27th in northern Taiwan, but the flow speed was similar at KHC between these two days. Surface meteorological data and sounding, including wind and temperature, were supported by the Central Weather Administration (CWA) and the Air Force Meteorological Wing (AFMW). Several ambient air quality monitoring stations have been established by the Ministry of Environment (MOENV) within the Taiwan area (Fig. 1). In addition, Aerosol Optical Depth (AOD) is one of the

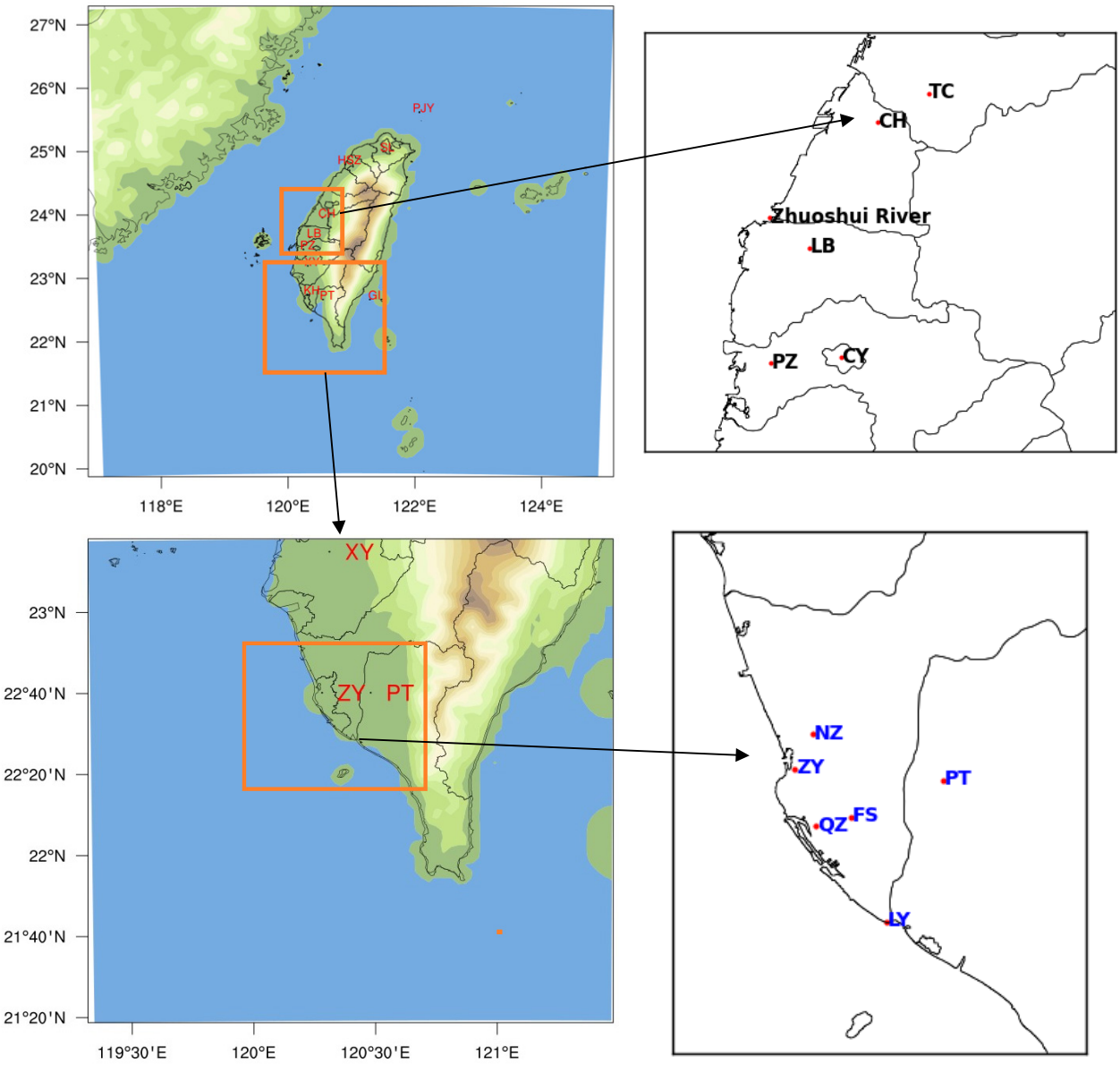

Fig. 1. (a) WRF simulation d01; (b) d02, including distribution of terrain; (c) southern Taiwan; (d) central Taiwan location of air quality monitoring and weather stations. The abbreviations of the measuring stations are Pengjiayu (PJY), Shillin (SL) in Taiepi (TP), Hsinchu (HSZ), Taichung(TC), Changhua (CH), Lunbei (LB), Chiayi (CY), Puzi (PZ), Xingying (XY), Kaohsiung city (KHC), Nanzi (NZ), Zuoying (ZY), Qianzhen (QZ), Linyin (LY), Fengshan (FS), Pingtung (PT), and Green Island (GI) and Zhuoshui River (ZSR).

most important quantities for aerosols (Chan, 2017; Sabetghadam *et al.*, 2021, 2018). AOD with ten-minute and hourly time resolution provided by CWA serves as a measurement for detecting dust.

There is a close relationship between density current and the ability of cold air to climb over the mountains. In understanding whether the northeasterly wind has the ability to climb over the central mountain range, the Froude number (Fr), which represents the energy that can be used for climbing over high hills, can be measured. Fr can be defined as the ratio of the momentum energy to potential energy like the relationship shown below:

$$F = \frac{U}{NH} \tag{1}$$

where

Fr: Froude number.

U: Flow speed across the mountain (m s^{-1}).

N: Brunt-Vaisala frequency (s^{-1}).

H: Height of mountain (m).

When Fr $\geq$ 0.5, it means that the airflow has the ability to climb a mountain. In contrast, when Fr $<$ 0.5, it indicates that the airflow cannot climb the mountain.

When the cold air flow cannot cross the mountain, the cold air stacks up behind the mountain to raise the pressure. Consequently, when the cold air pressure gradient accumulates to overcome the height of the mountain and crosses the mountain, it produces a fast-moving air flow that transports PM southward. The speed of the transport is shown in Eq. (2) (Houze, 1993; Crouvi *et al.*, 2017). Density current speed is represented as Ud

$$U_d = F\sqrt{gh\frac{\rho_1 - \rho_2}{\rho_1}} \tag{2}$$

where

F: Dimensionless densiometric Froude number.

g: Acceleration due to gravity

ρ_1: Cold air density at Position 1.

ρ_2: Warm air density at Position 2.

h: the thickness of the gravity current (m).

2.2 WRF Modeling Parameter Setting and Results Verification

The WRF model was used to simulate meteorological factors from January 26–27, 2018 (China Standard Time). The model runs 6 hours as spin-up time. The outermost domain (D1) has a horizontal grid of 90 × 90 and a grid spacing of 9 km, which covers southeastern China and Taiwan with a domain center point at 25°N, 120°E. Domain 2 (D2), covering the area of southern Taiwan, has a horizontal grid of 73 × 73 and a grid spacing of 3 km. The model's vertical level is 43 and initial meteorological fields and boundary conditions were adopted from NCEP FNL Operational Global Analysis Data with 1° × 1°-resolution-degree grids for every 6 hours. The common model physics options included: WSM5 microphysics scheme (Hong *et al.*, 2004), shortwave radiation for Dudhia scheme (Dudhia, 1989), RRTM longwave radiation schemes (Mlawer *et al.*, 1997), Kain-Fritsh cumulus scheme (Kain and Fritsch, 1993), the 5-layer thermal diffusion scheme (Dudhia, 1996) for land surface model (LSM), and YSU PBL scheme (Hong, 2010; Hong *et al.*, 2006), which could be useful for air pollution dispersion studies (Boadh *et al.*, 2016). According to Alizadeh Choobari *et al.* (2012), different PBL schemes might have impacted dust transport. This article also conducted sensitivity analysis on the Mellor-Yamada-Janjic scheme (MYJ). The correlation coefficient between YSU and MYJ in surface temperatures exceeds 95%. Since these two different schemes were not sensitive to temperature simulation results in this case, the article only analyzed the results of the YSU scheme simulation.

Quantitative comparisons between WRF and observations were based on the Mean Bias Error (MBE), the Mean Absolute Bias Error (MAE), and the Root Mean Square Error (RMSE). The MBE, MAE, and RMSE are computed as follows:

$$MBE = \frac{1}{n}\sum_{1}^{n}(M - O) \tag{3}$$

$$MAE = \frac{1}{n}\sum_{1}^{n}|M - O| \tag{4}$$

$$RMSE = \sqrt{\frac{\sum_{1}^{n}(M-O)^2}{n}} \quad (5)$$

where M and O represent the modeled and observed values of the variables, respectively, and n is the number of data.

In general, the verification results indicate that the WRF model can simulate the surface observed trend in KHC and Pingtung county—Pingtung (PT), Nazi (NZ), Linyin (LY) average (Table 1). The model verification was conducted after a six-hour spin-up using the YSU scheme and the simulated surface temperature MB was –1.09°C and –1.70°C on January 26 and 27, 2018, respectively, which was similar to –1.04°C by Boadh *et al.* (2016) and –1.88°C by Fekih and Mohamed (2019). The simulated surface relative humidity MAE was 8.57% and 8.16% on January 26 and 27, 2018, respectively, which was similar than 9.72% by Boadh *et al.* (2016). The simulated surface wind speed RMSE was 2.10 m s^{-1} and 1.8 m s^{-1} on January 26 and 27, 2018, respectively, which was similar to 2.02 m s^{-1} by Madala *et al.* (2015). Notably, the calibration data of WRF models with the observations are reasonable.

This study used model data to estimate the density current speed and air parcel trajectories to verify the consistency between the density current and PM_{10} transport speeds. However, this study has its limitations. Due to the wave-like behavior and rapid transport speed of density

Table 1. Statistical evaluation of surface meteorological variables between WRF simulated and observation.

Time	2018 Jan. 26th			2018 Jan. 27th		
statistical comparison	MB	MAE	RMSE	MB	MAE	RMSE
Temperature (°C)	–1.09	1.47	1.73	–1.70	2.50	2.90
Relative Humidity (%)	6.27	8.57	9.67	8.06	8.16	9.04
Wind speed (m s^{-1})	1.62	1.72	2.10	1.85	1.90	1.88
	Hong *et al.* (2006)			Hariprasad *et al.* (2014)		
statistical comparison	MB	MAE	RMSE	MB	MAE	RMSE
Temperature (°C)	< 0.5		2–2.5		0.86	1.03
Relative Humidity (%)				–14.54	14.67	16.18
Wind speed (m s^{-1})				0.74	1.1	1.33
	Madala *et al.* (2015)			Boadh *et al.* (2016)		
statistical comparison	MB	MAE	RMSE	MB	MAE	RMSE
Temperature (°C)	0.29		1.67	–1.04	1.56	1.93
Relative Humidity (%)	2.2		12.75	4.66	9.72	12.41
Wind speed (m s^{-1})	–1.4		2.02	0.33	0.78	1.04
	Hung *et al.* (2018)			Fekih and Mohamed (2019)		
statistical comparison	MB	MAE	RMSE	MB	MAE	RMSE
Temperature (°C)	–0.78	2.58	4.18	–1.88		2.76
Relative Humidity (%)						
Wind speed (m s^{-1})	2.13	2.49	3.16	–1.18		2.35
	Tsai *et al.* (2020)			Li *et al.* (2022)		
statistical comparison	MB	MAE	RMSE	MB	MAE	RMSE
Temperature (°C)	0.2	0.9		–0.98		3.35
Relative Humidity (%)				5.99		17.44
Wind speed (m s^{-1})	0.5		1.4	2.10		2.62
	Souza *et al.* (2023)			Kartsios *et al.* (2024)		
statistical comparison	MB	MAE	RMSE	MB	MAE	RMSE
Temperature (°C)				–0.09		2.62
Relative Humidity (%)						14.98
Wind speed (m s^{-1})	0.82		2.09			3.9

currents, hourly surface observational data cannot fully capture the speed of these currents. In the future, high-resolution surface observations and upper-air observational data will be needed to conduct a more in-depth analysis of the effects of density currents on PM_{10} transport.

3 RESULTS AND DISCUSSION

3.1 Synoptic Flow and Terrain Interaction on Kaohsiung's High PM_{10}

Fig. 2 shows the weather maps for the islands of Taiwan and its surrounding area, the 1032 mb sea level pressure contour reached 30°N of Mainland China at about 0800 LST on January 26, 2018. The PGF between Taiwan and 30°N of China was significant in inducing a strong northeasterly blow toward Taiwan. However, the pressure gradient began to decline after 0800 LST on January 27, 2018, and the northeasterly wind decreased its strength as well.

The first potential impact of a northeasterly invasion in Taiwan is producing speedy winds on its northeastern part, the frontline for northeasterly blows. Not only was there about a three to fourfold difference in the surface wind speeds between northern and southern Taiwan, but the cold air also declined its strength while moving southwardly.

In addition, effects can include creating heavy fugitive dust from dry floodplains of rivers, especially during drought seasons (Lin *et al.*, 2018; Kuo *et al.*, 2017; Lin *et al.*, 2016; Kuo *et al.*, 2014, 2010). Highly speedy winds may also transport air pollutants away from their origins with the movement of density current (Crouvi *et al.*, 2017), which is particularly focused on in this study.

Figs. 3(a) and 3(b) demonstrate PM_{10} concentration variation patterns detected by two represented air quality monitoring stations, Zuoying (ZY) and Fengshan (FS) of KHC, during the 48 hours from January 26 to 27, 2018. The PM_{10} concentration variation pattern on January 27, 2018, was at a "usually high" level and normally peaked near noon (Li *et al.*, 2017). However, the PM_{10} concentration on January 26, 2018, as shown in Fig. 3(a), for this study was kept at a high level of about 70–80 μg m^{-3} from midnight to 1500 LST initially. Subsequently, it was increased to a crowning concentration near 180 μg m^{-3} on the evening of January 26, 2018. PM_{10} returned to its "usually high" concentration after 2200 LST on January 26 and continued decreasing on the 27th.

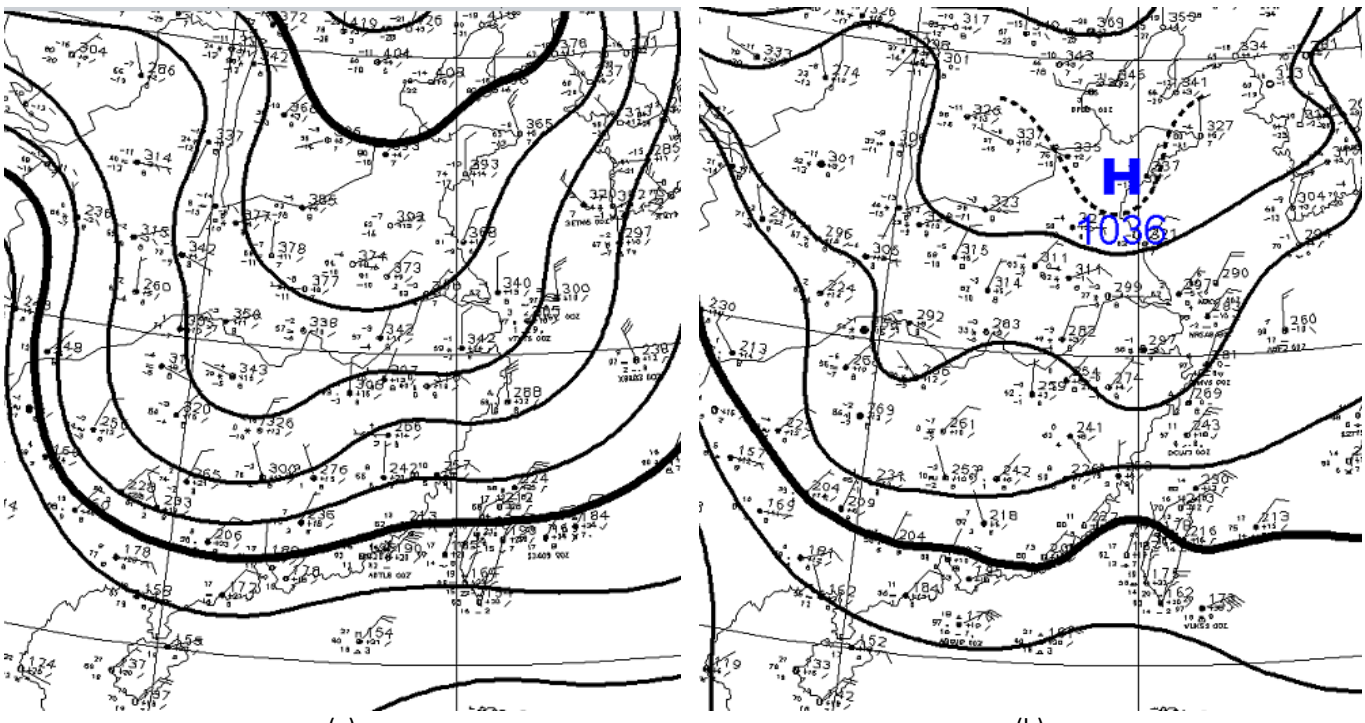

(a) (b)

Fig. 2. (a) Sea level pressure and surface wind on January 26, 2018, at a 0800 LST sea level pressure and (b) 27 at 0800 LST.

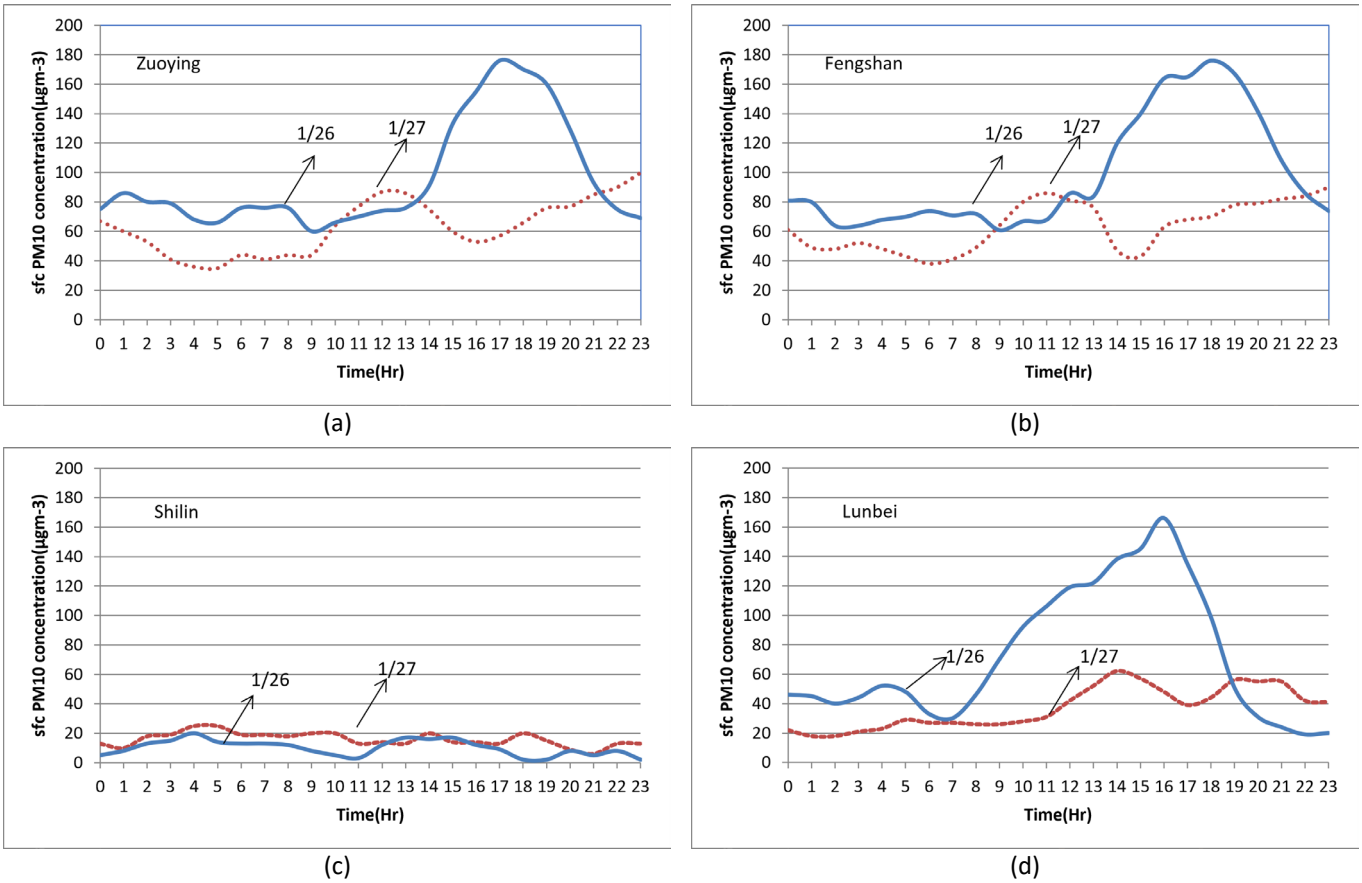

Fig. 3. The time series of PM_{10} on the 26th (blue line) and the 27th (red dot line) at (a) Zuoying, (b) Fengshan, (c) Shilin, and (d) Lunbei.

KHC's PM_{10} concentration was much higher than the PM_{10} concentration at Shilin (SL) in northern Taiwan (Fig. 3(c)). Thus, KHC's high PM_{10} concentration was not transported from northern Taiwan. Meanwhile, the maximum PM_{10} concentration in midwestern Taiwan was high—for example, that of Lunbei (LB), was above 140–160 μg m^{-3} at 1400 LST (Fig. 3(d)). The high PM of KHC might be related to the leeward side effect. However, LB is located in the ZSR downstream, 15 km south of ZSR, where the river dust could transport PM_{10} downstream, affecting the air quality of LB.

In establishing the flow fields, the flow field near Green Island (GI) (Fig. 4(a) dot red circle) was used as an example to indicate the flow pattern of the northeasterly winds before arriving in Taiwan. Fig. 4(b) depicts the wind speeds in the atmosphere above GI up to 2000 m in height, which indicates the strongest wind occurring at the position of 700 m above ground with a speed of about 17 m s^{-1} at 0800 LST on January 26, 2018. Until the evening of January 26, the northeasterly winds below 1000 m were still significantly high and continued to the evening the next day. At 0800 LST on January 27, strong winds were found below 700 m in height. It was not until 2000 LST on January 27 that the wind speed reduced to less than 8 m s^{-1}. The variation of the wind speeds during these two days followed the invasion pathways of the northeasterly blow—that is, the northeasterly blow approached Taiwan on the morning of January 26, 2018, and had the highest wind speed on the evening of January 26. The wind remained at high speeds until the evening of January 27, 2018.

Based on the values provided by the observational sounding data around the GI and altitudes of the southern mountains of CMR, according to (1) for Fr = U/NH, H was about 2000 m, and N was equal to 0.01 s^{-1}. The angle between the northeasterly wind direction and the north-south axis of the mountain range was about 20–30 degrees on January 26 and 27, 2018. For southeastern Taiwan, U was taken using the highest wind speed of 8.5 m s^{-1} (= 17 m s^{-1} × sin 30°) for January 26. At 0800 LST and 2000 LST on January 27, U values were considered 7.5 m s^{-1} (= 15 m s^{-1} × sin 30°) and 3.0 m s^{-1} (= 6 m s^{-1} × sin 20°), respectively.

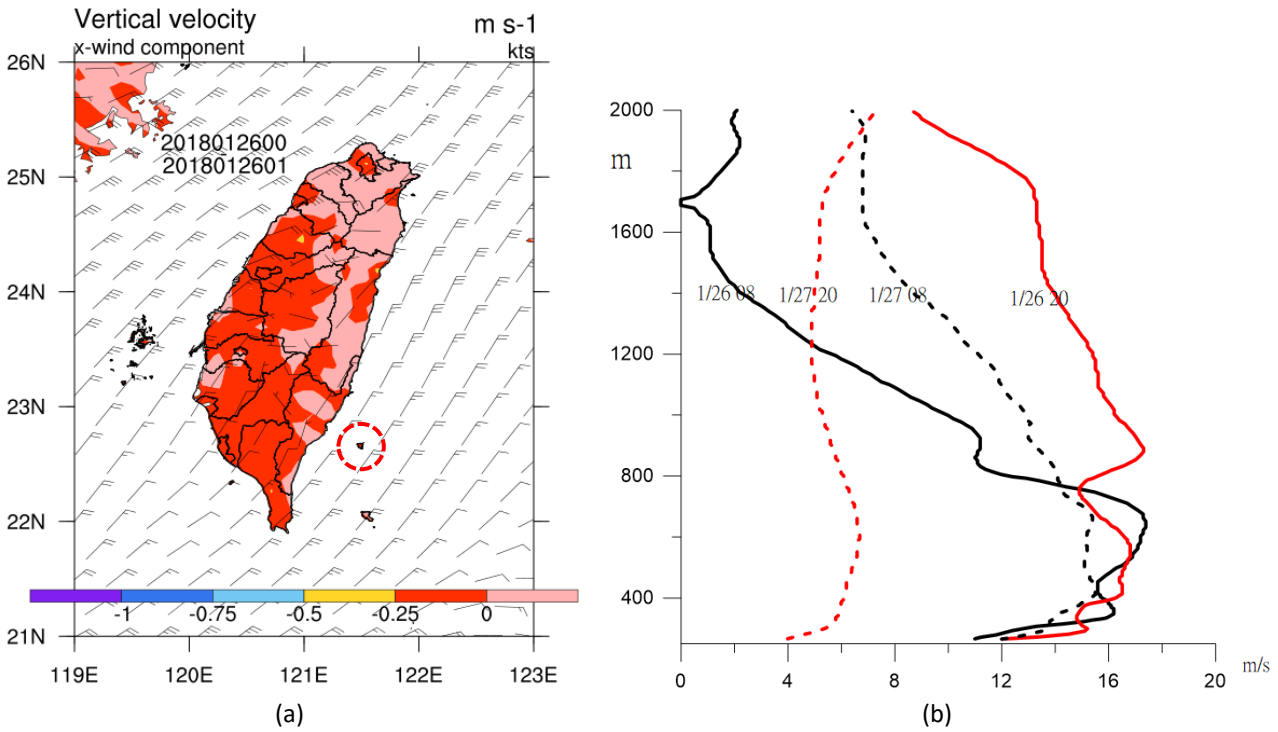

Fig. 4. (a) Observational wind vector at 800–900 m and vertical velocity at the surface on January 26, 2018, at 0800 LST; (b) wind profile on January 26 at 0800 LST (black line) and at 2000 LST (red line), on January 27 at 0800 LST (black dash line) and at 2000 LST (red dash line) at Green Island (dash red circle) in Fig. 4(a).

The Fr number for southeastern Taiwan during these two days ranged from 0.15 to 0.4 (Table 2). This result indicates that the flows were unable to climb over the CMR owing to the Fr number below 0.5. Although the northeasterly winds seemed strong, the angle between the wind flow direction and the mountain lines was too small to allow the current flows to pass over CMR. However, the Fr number of northeastern Taiwan ranged from 0.45 to 0.7 on January 26, which could indicate whether the flows were nearly critical to climb over the CMR or not. As the flow passed the northeastern mountain and induced subsidence warming, the large temperature contrast and pressure gradient from central Taiwan to northern Taiwan increased, such that large horizontal pressure contrast would favor the condition of the density current. Although the southeastern flow could not pass the mountain, the subsidence over KHC existed owing to the large-scale downward motion (Fig. 5).

The two temperature inversion levels in the atmosphere of southwestern Taiwan on January 26, 2018, were observed (Fig. 5(a)). The near-ground lower inversion level generally resulted from ground radiation effects, which usually more critically inhibit a vertical movement of air pollutants in the near-ground atmosphere (Sun *et al.*, 2019; Wallace and Kanaroglou, 2009; Zhang *et al.*, 2009). Furthermore, the upper inversion level might have resulted from atmospheric subsidence, probably due to the invasion of high pressure (Largeron and Staquet, 2016; Xu *et al.*, 2019).

Table 3 summarizes both positions of inversion levels and PBLH at the PT station on January 26 and 27, 2018. Based on the observed temperature profiles, the lower inversion level was at about 300 m above ground, while the upper inversion level was at 650 m above ground at 0800 LST on January 26. However, the lower inversion level was further reduced to 250 m above ground, while the upper inversion level was raised to 950 m above ground at 2000 LST. In contrast, on January 27, the lower inversion level remained below 300 m, while the upper inversion level was at about 850 m above ground at 0800 LST. At 2000 LST on January 27, only one inversion level above 1000 m was detected, and no lower inversion level was observed. It was found that the mixing zone was not high enough to dilute air pollutants in the near-land atmosphere for the two days despite the atmospheric temperature structures returning to their usual conditions on the evening of January 27.

Table 2. Atmospheric characteristics for January 26 and 27, 2018.

Date	01/26/2018		01/27/2018	
PBLH at Pingtung	0800 LST	2000 LST	0800 LST	2000 LST
Lower inversion level	300 m	250 m	250 m	–
Higher inversion level	650 m	950 m	850 m	> 1000 m
PBLH	212 m	313m	243 m	> 500 m
Fr on southeast/northeast Taiwan	0.4/0.45–0.7	0.35/0.7	0.35/0.5	0.15/0.37
Typical PM_{10} concentration of ZY station	76 μg m^{-3}	129 μg m^{-3}	44 μg m^{-3}	77 μg m^{-3}
PGY wind speed	15.3 m s^{-1}	13.9 m s^{-1}	10.8 m s^{-1}	7.5 m s^{-1}
ZY wind speed	2.5 m s^{-1}	3.2 m s^{-1}	1.8 m s^{-1}	1.9 m s^{-1}
Major causing mechanisms for high-concentrated PM_{10}	PBLH and density current			

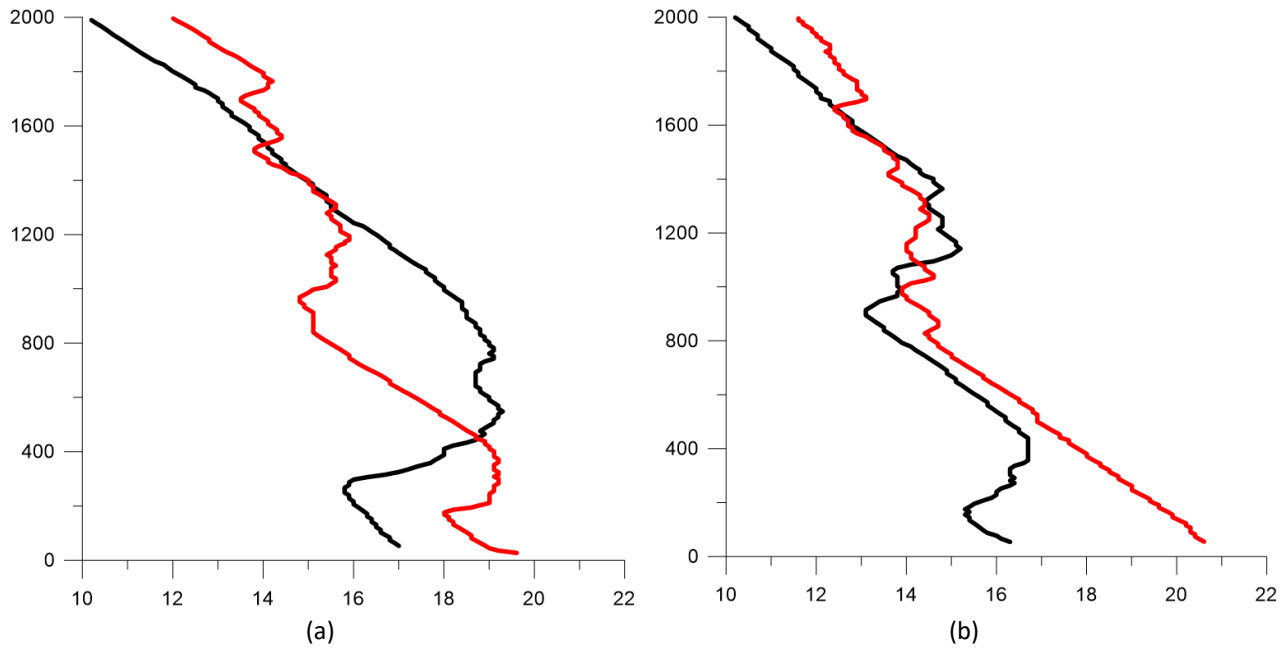

Fig. 5. Observational temperature profile (°C) at Pingtung from January 26–27, 2018: (a) the dark line was (a) on the 26th at 0800 LST, and the red line was on the 26th at 2000 LST; (b) the black line was on the 27th at 0800 LST, and the red line was on the 27th at 2000 LST.

3.2 River Dust and Density Current Effect on Kaohsiung's High PM_{10}

Table 3 shows the PM_{10} concentration evolution of selected ambient air quality monitoring stations from middle to southern Taiwan on January 26, 2018, which was selected for further analysis. Both the highest concentrations of PM_{10} and its peak time for these stations are tabulated and summarized as follows: 250 μg m^{-3} peaked at 1400 LST in Puzi (PZ), located in the Chiayi county, 162 μg m^{-3} peaked at 1600 LST in Xingying (XY), located in Tainan, and 163 μg m^{-3} peaked at 1800 LST in Quinzhen (QZ) located in KHC. As shown in Fig. 6(a), observations from the air quality monitoring stations, including PZ, XY, and QZ, demonstrated a typical long-range transportation of PMs. The transportation of air-born particles was of particular concern in this study.

In terms of possible typical southward transportation pathways for PMs, Changhua (CH) PM_{10} was 82 μg m^{-3} peaked at 1600 LST, was located upstream, while the rest of the three stations were located downstream with a position of LB, PZ, and XY. They are separated by the CSR. It was found that the wind speed at LB was above 6.5 m s^{-1} from 0700 LST to 1800 LST on January 26, 2018 (Table 3), which was strong enough to remove sand dust from drought riverbeds. Therefore, we hypothesized that the high-concentrated PM_{10} at LB might be contributed by the sand dust from the nearby river, the CSR in this case. The sandstorm affected LB first and was brought to PZ later. It was further transported southwardly to XY and even more southwardly to KHC.

Table 3. PM_{10} peaking time, the maximum hourly average wind speed of the day, the accompanying average wind speed in the last ten minutes and gust wind for January 26, 2018.

First time PM_{10} rapidly increases (doubles in one hour) at LB	wind speed $\geq$ 6.5 m s^{-1}	Peak PM_{10} concentration ($\mu g\ m^{-3}$)	PM_{10} peaking time on Jan. 26, 2018
0700 LST	0700–1800 LST	166	1600 LST
$PM_{10} \geq 150\ \mu g\ m^{-3}$ of ambient air quality monitoring stations	Maximum hourly average wind speed of the day/Average wind speed in the last ten minutes/Gust wind	Peak PM_{10} concentration ($\mu g\ m^{-3}$)	PM_{10} peaking time on Jan. 26, 2018
PZ (in CY)	4.8 m s^{-1}/6.0 m s^{-1}/9.3 m s^{-1} (in CY)	PZ 250	1400 LST
XY (in TN)	4.4 m s^{-1}/5.3 m s^{-1}/13.4 m s^{-1} (in TN)	XY 162	1600 LST
TN (in TN)	3.9 m s^{-1}/5.2 m s^{-1}/13.4 m s^{-1} (in TN)	TN 305	1600 LST
ZY (in KHC)	4.3 m s^{-1}/5.1 m s^{-1}/9.3 m s^{-1} (in KHC)	ZY 176	1700LST
QZ (in KHC)	2.6 m s^{-1}/2.6 m s^{-1}/9.3 m s^{-1}(in KHC)	QZ 163	1800 LST

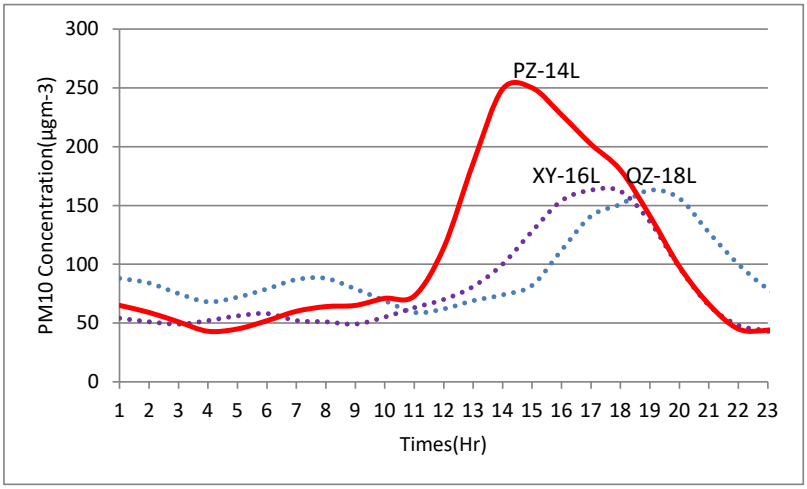

(a)

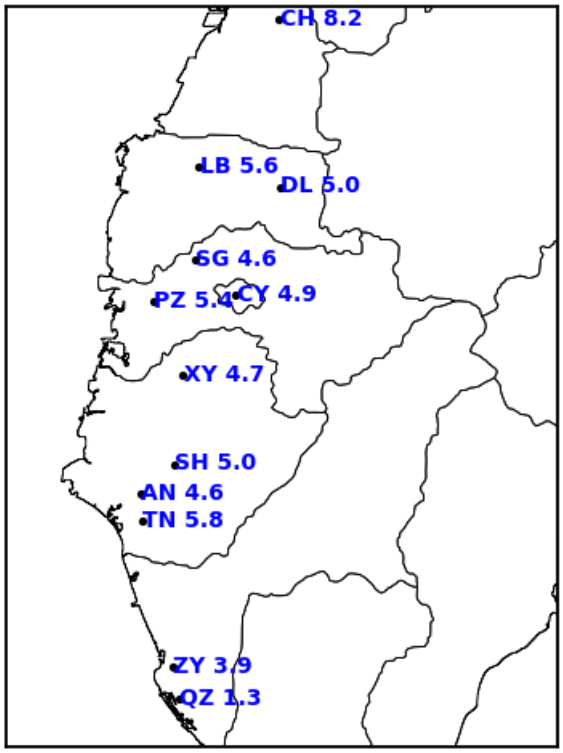

(b)

Fig. 6. On January 26 2018 (a) the time series of PM_{10} ($\mu g\ m^{-3}$) at Puzi (PZ: red), Xinying(XY: dot purple), and Qianzhen (QZ: dot blue) by observation (the number marked on the right side of the measuring station is the PM_{10} peaking time) and (b) 1600 LST hourly average wind field at surface stations (CN, LB, PZ, XY, TN, ZY, QZ) and additional stations as Douliou (DL), Singang (SG), Shanhua (SH), Annan (AN).

Notably, the surface wind speed at PZ was only about 5 m s^{-1}. In addition, with about a 116 km distance from Chiayi's PZ to KHC's QZ, the peak concentration of PM_{10} for PZ occurred at 1400 LST and that for QZ occurred at 1800 LST. If this peak concentration of PM_{10} in KHC came from Chiayi's PZ, its transmission rate should be higher than 8 m s^{-1} to arrive in KHC at 1800 LST. However, Fig. 6(b) and Table 3 showed that surface hourly wind speed and average wind speed in the last ten minutes were lower than those in PM transport speed. For example, the highest wind speed at PZ was only 5–6 m s^{-1}. All these findings suggest that the movement of the air parcels transporting along the west side of the CMR cannot be captured by surface average winds. According to density current wave behavior, only the density current flows have the potential to make the air parcel move quickly.

However, density current needs high temporal resolution of meteorological measurements to capture its characteristics (Evan *et al.*, 2022). High temporal resolution of AOD was analyzed to verify the evidence of density current. Fig. 7 showed that in 1100 LST AOD thickness at LB and PZ was thicker than that in 0900–1000 LST. The increase in PM_{10} at LB from 0800–1200 LST was nearly three times, which was consistent with the AOD thickening trend during this period. And CY' AOD became significant at 1100 LST (Fig. 7(c)), which was one hour later after LB's AOD occurred. Meanwhile, at 1100 LST the PM_{10} in PZ (in CY) from 1000 to 1200 LST ranged from 73 μg m^{-3} to 186 μg m^{-3}. The relationship between AOD and PM_{10} was significant, and AOD time evolution

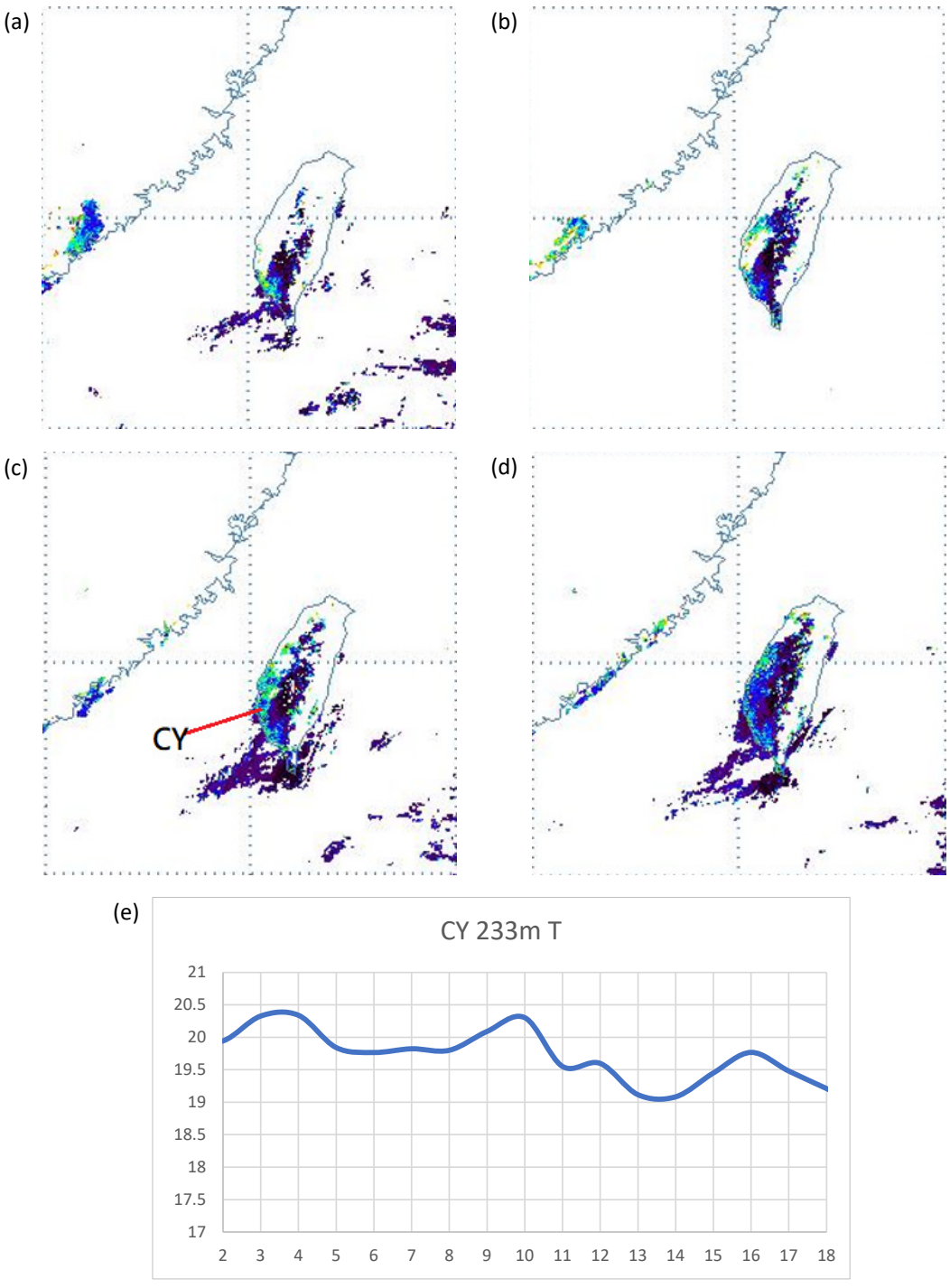

Fig. 7. AOD at (a) 0900 LST, (b) 1000 LST, (c) 1100 LST, and (d) 1200 LST and (e) simulated 233 m temperature (°C) on January 26, 2018.

represented the density current behavior. In addition, the model simulation of CY's temperature at 233 meters above the ground showed wave propagation. Both observations and models showed that there was a density flow phenomenon in this case.

Fig. 8(a) shows the surface temperature in Hsinchu (HC) in the north of Taiwan and Chiayi (CY) in central-southern Taiwan. Except for a slight rise at noon, the surface temperature in HC continued to fall over time. However, in Chiayi, the surface temperature continued to rise after sunrise. The horizontal temperature gradient between Chiayi and Hsinchu was above 3°C from 9 a.m. to 5 p.m. This surface temperature gradient induced the pressure difference in these two places, reaching as high as 3 mb and increasing after 0600 LST (Fig. 8(b)). This gap in the atmospheric pressure induced the density difference and might even produce the formation of density current flows on the west side of CMR, which would make air-born PMs to move quickly. It was estimated to take about 1.5 hours for PMs to be transported through surface winds from LB to PZ with a reported wind speed of 8 m s^{-1} and a distance between them of about 42 km. These PMs would keep transporting into Taiwan's XY.

According to Eq. (2) in calculating the density current speed, the yielded densities ρ_1 and ρ_2 would be 1.2 kg m^{-3} and 1.184 kg m^{-3}, respectively, since the PZ surface temperature was 19.3°C, with a pressure of 1012.4 hPa at 1400 LST and the QZ surface temperature was 24.1°C at 1400 LST with a pressure of 1010.7 hPa. The calculated density current flow speed, U_d, ranged from 8 to 12 m s^{-1}, which depends on whether H varied from 300 m to 600 m, which was near 8 m s^{-1} and was more reasonable for transporting PM_{10} quickly along the west side of CMR.

Both peak PM_{10} concentrations for Chiayi—PZ and KHC—CZ occurred at 1400 LST and 1800 LST, respectively. The forward trajectory for air parcel in northeastern Taiwan and the backward trajectory for the air parcel of KHC indicate the air flows coming from northern Taiwan (Figs. 9(a), 9(b)). Hence, when taking a KHC air parcel at 1800 LST as an example, the trajectory moved in 158 km from the ZSR to KHC for five hours. It was estimated that the backward trajectory position at 1300 LST was closely located in ZSR (Fig. 9(b)), and the average traveling velocity from the ZSR was as fast as 8 m s^{-1}, which is consistent with the speed of the density current.

Under a stable atmosphere, as northeasterly reached CMR, and was blocked on the wind side of the terrain, and was accumulated to high density of air. This phenomenon formed a significant horizontal density gradient and PGF between the leeward and the wind side of the terrain (Fig. 10). The density gradient provided the environment of density current, as strong PGF push air flow moved southward, under a stable atmosphere, air flow formed density current as shown in Fig. 11. Air flow was forced by significant PGF (Fig. 11(a)), the cold air moved southward and was stimulated into a density current (Fig. 11(b)). Behind the first cold air, the second cold air was still induced by PGF, forming a density current (Figs. 11(c) and 11(d)). In calculating the speed of the density current—from 1400 LST to 1600 LST—with the cold air moving above 60 km, the average flow speed was about 9–10 m s^{-1}, which was similar to PM_{10}'s transporting speed.

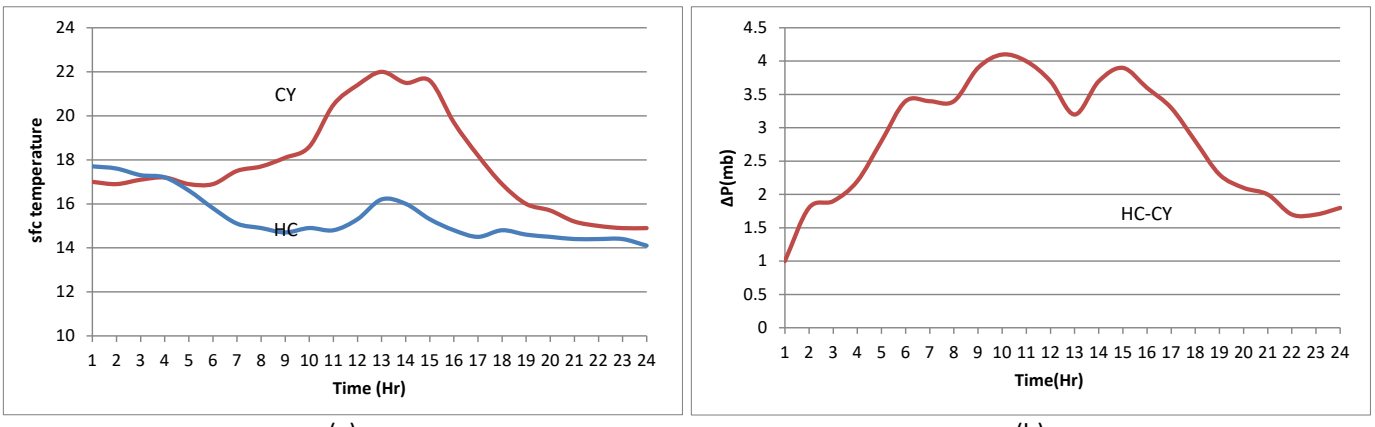

(a) (b)

Fig. 8. The time series of (a) surface temperature at Chiayi (CY) (red line) and Hsinchu (HC) (blue line) and (b) sea level pressure difference of Hsinchu (HC) minus Chiayi (CY) on January 26, 2018.

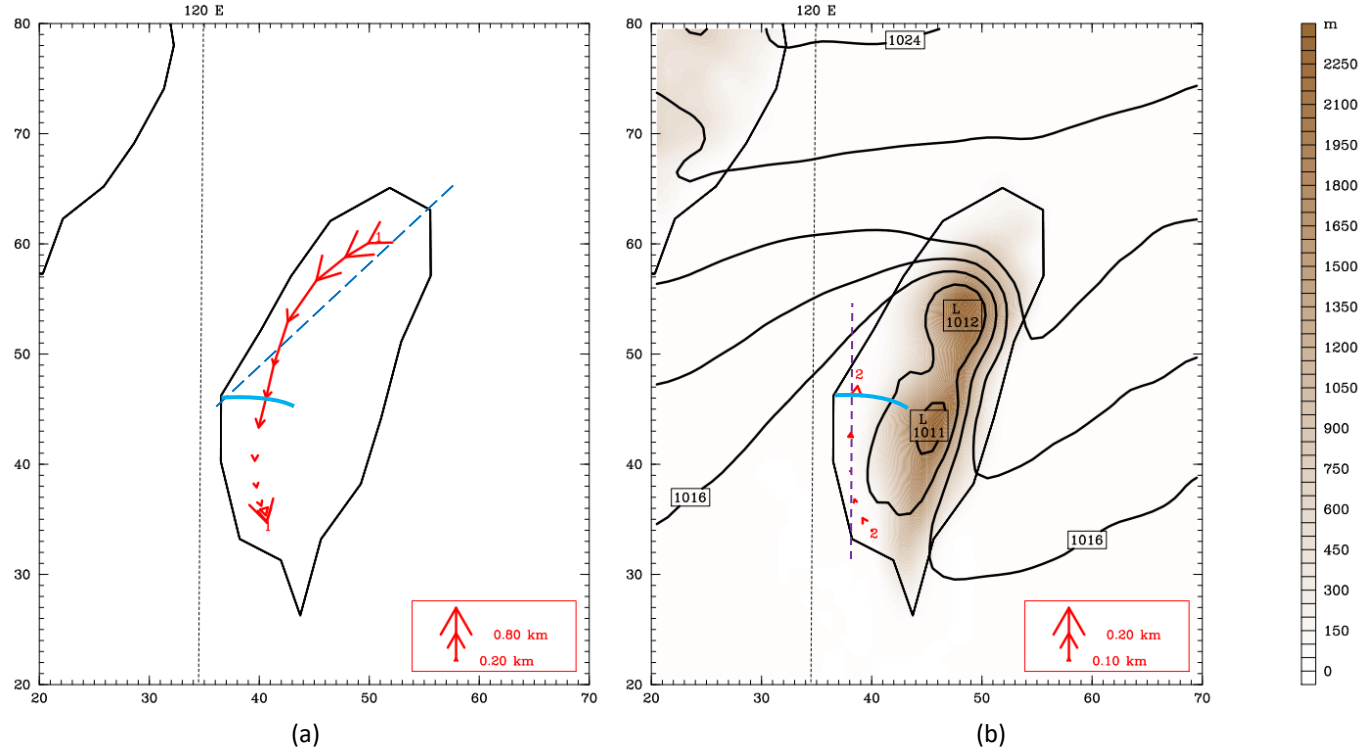

Fig. 9. The forward trajectory (a) from 0200 LST to 1400 LST on January 26, 2018 (the blue line represents the location of the ZSR; the blue dash line represents Fig. 10's cross-section (35,45)–(55,67)); (b) the backward trajectory from 1800 LST to 1300 LST on January 26, 2018, and sea level pressure at 1400 LST on January 26, 2018. Brown shading represents the height of the terrain, while the purple dotted line represents Fig. 11's cross-section.

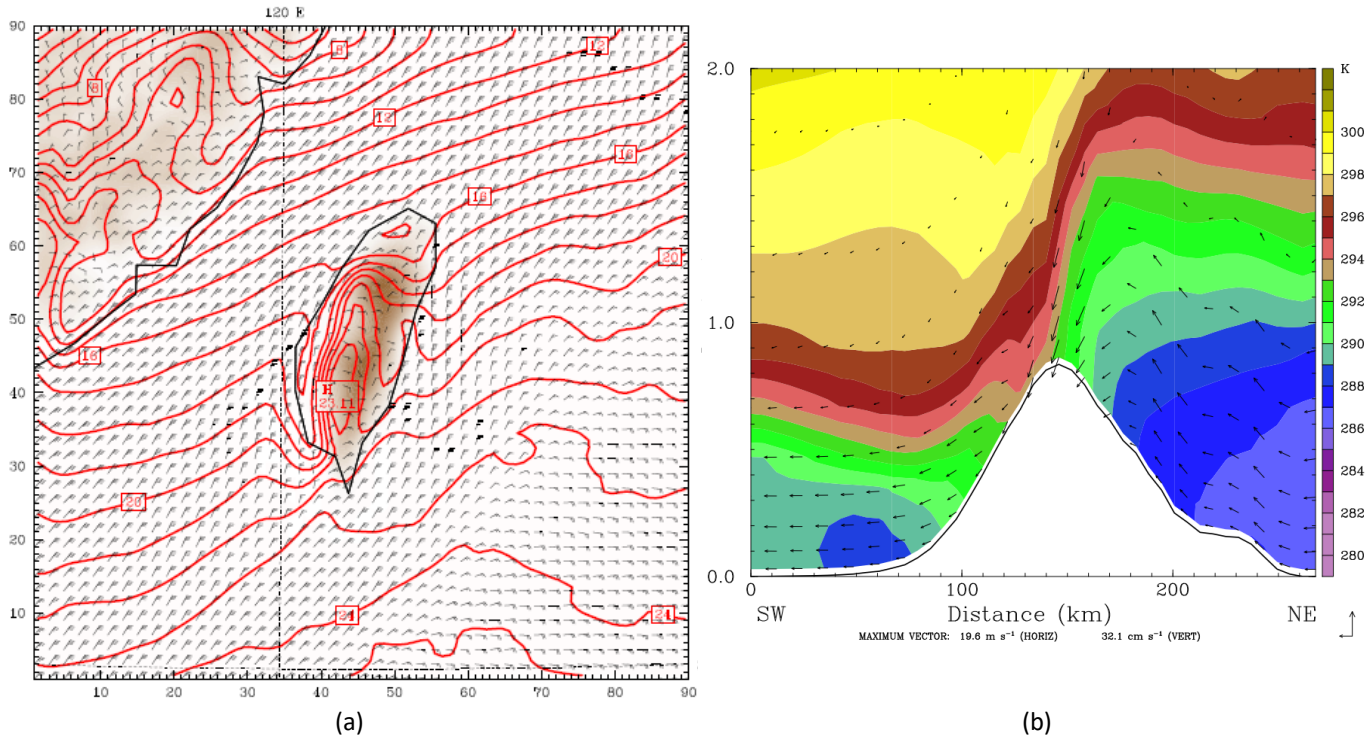

Fig. 10. The simulated (a) surface temperature (°C) and (b) uw circulation and potential temperature in the northeast-southwest vertical profile in Fig. 9(a) (35,45)–(55,67) at 0800 LST on January 26, 2018.

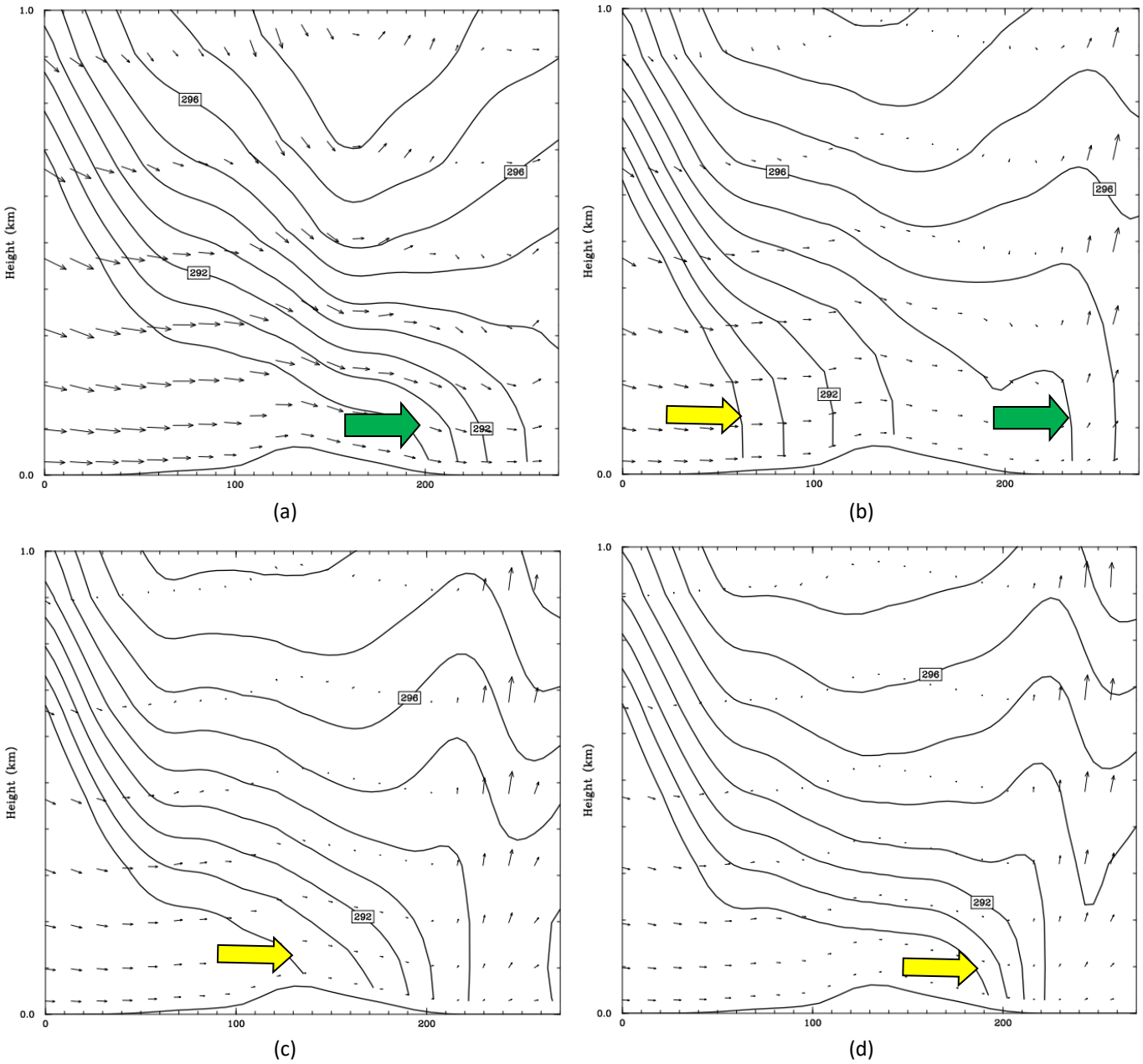

Fig. 11. The simulated uw circulation and potential temperature in the Y–Z profile in Fig. 9(b) (38,55)–(38,25) at (a) 0800 LST, (b) 1400 LST, (c) 2000 LST on January 26, 2018, and (d) 0200 LST on January 27, 2018. Green and yellow arrows represent the different flows.

The formation of density currents on the west side of Taiwan requires a significant density difference between the north and south of western Taiwan. Fig. 10(b) shows that the cold air in the windward area of the mountain ranges was stacked up, and there was warm air owing to subsidence inversion (Figs. 12(a) and 12(b)) in the leeward area. Meanwhile, after sunrise, the sun heated the air near the ground, resulting in an increase in the temperature in the west of central and south of Taiwan. However, in the northern part of Taiwan—owing cold advection of the Northeastern Monsoon coupled with the topography of the obstacle—there was no significant warming of the northern part of Taiwan, resulting in the case of the north-south temperature difference.

This article shows the conditions for the generation and transport of dust in rivers and the process of dust transport to the southern Taiwan. This has some similarities with the process of

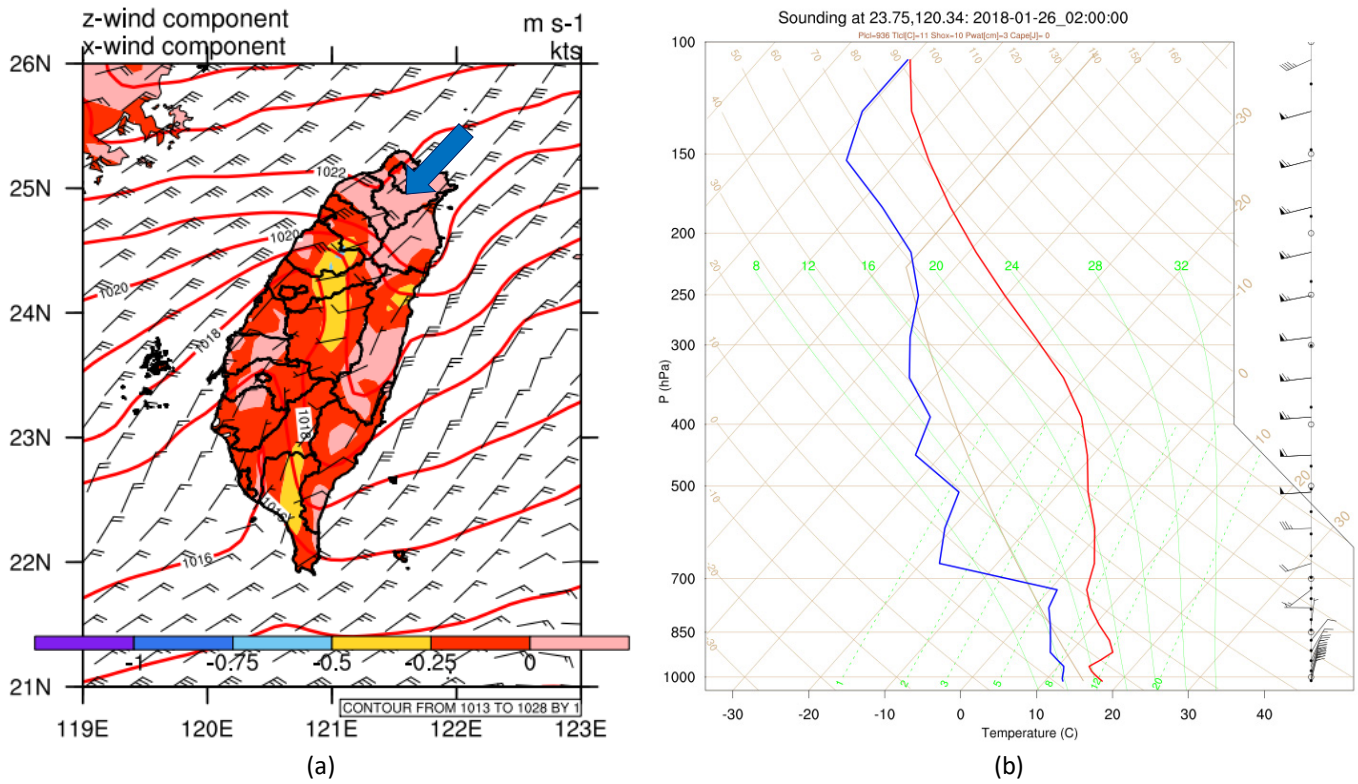

Fig. 12. The simulated (a) sea level pressure (mb), surface wind vector and vertical velocity (cm s^{-1}) at 300 m and (b) LB skew logT-P on January 26, 2018, at 1000 LST. Heavy blue arrow represents the wind direction.

Asia dust storms (Chen and Chen, 1987; Parrington *et al.*, 1983; Park *et al.*, 2010; Shaw, 1980; Zhang *et al.*, 2018; Zhang *et al.*, 2017). When WAM is significant, strong surface flow and low humidity in the lower troposphere over arid areas of China or Taiwan' river become the most favorable conditions for the generation of dust. These potential adverse effects impacts on ambient air quality—which may include enhancing transportation of Asian dust or Taiwan river—particularly concern people living in the southwestern part of Taiwan (Lin *et al.*, 2004; Li *et al.*, 2017; Park *et al.*, 2010).

Long-range dust transport in Asia may occur through strong PGF accompanied by WAM. However, the PGF between central and southern Taiwan is weak. In calculating the speed by PGF acceleration, at 1300 LST the TC sea level pressure is 1016.9 hPa, the CY sea level pressure was 1016.5 hPa, and the density was 1.2 kg m^{-3}, resulting in an acceleration of 4×10^{-4} m s^{-2}. The velocity increase produced by one hour of acceleration was only 1.44 m s^{-1}. The wind speed was less than the propagated speed of PM_{10} in 8–10 m s^{-1}. Therefore, the transmission of dust from rivers in central Taiwan to the south is not only caused by PGF. The key process of rapid PMs propagation is due to interaction between WAM and CMR to stimulate density current, and subsidence inversion kept PM_{10} trapped near the ground.

To compare with Sun *et al.* (2019), who studied the interaction between Beijing's topography and cold air, both PGF and inversion play important roles in high PM levels. However, Sun *et al.* (2019) demonstrated that a significant PGF triggers easterly airflow, bringing dust masses to Beijing. Our article shows that the rapid increase in PM levels in the southern part of Taiwan was due to the formation of density flows in central and northern Taiwan, which then rapidly transported dust from the central part to the south of Taiwan.

4 CONCLUSIONS

In this paper, we analyzed the mechanism of density current generation and its possibility of

rapidly increasing PM_{10} in KHC through observational data and the WRF model. A significant PGF between northern and central Taiwan induced strong winds that blew river dust in central Taiwan and stimulated a density current transporting PM_{10} southward rapidly. AOD and WRF simulated temperature, trajectory provided information about density current behavior, and how the density current was formed. Some important findings from this investigation are summarized as follows:

1. The high PM_{10} in KHC was caused by long-range transporting. A significant PGF induced strong winds that blew river dust in central Taiwan under a stable atmosphere and stimulated a density current transporting PM_{10} to KHC. In calculating the speed of density current, it was set to 8 m s^{-1} to align with the PM's transporting speed.
2. The cold air on the windward side accumulates to a high pressure, a large north-south horizontal pressure gradient was formed in central western Taiwan between the cold flow originating from northern Taiwan and the warm flow by solar heating. As significant PGF push the flow, it stimulated a density current.
3. As cold air formed strong PGF to acclearate northeasterly flow above 10 m s^{-1}, the flow passed over the north of CMR, and produced subsidence warming in central Taiwan, located on the leeward side of northeastern CMR.
4. The inversion between central and southern Taiwan traps PM_{10} near the ground, as the density flow was driven, it caused a rapid increase in PM_{10} in the central and southern Taiwan. After PM_{10} was transported into KH efficiently in a short time by the density current, the local effect of weak rear flow and subsidence in KH enhanced and maintained PM even more than it did in central Taiwan.

Although this article applied AOD and WRF simulation results to show density currents rapidly transport PM_{10} southward, we also demonstrated the limitations of observational data. The first is lack of high time resolution to catch density current speed, even hurly average wind speed or the ten-minute average wind speed. The second is lack of sounding between central and southern Taiwan to direct observation on vertical structure of density current. Although some intensive observational periods have been held in central and southern Taiwan in recent years, river management administration in central Taiwan have spent much efforts to reduce high river dust pollution events. However, future work will continue to focus on analysis of PMs events suitable for intensive observation periods and model simulation including chemical reaction. By understanding the physical process of PMs transmission, to make more reliable predictions of changes in air pollution and reduce the damage of high pollution to economic activities.

ACKNOWLEDGMENTS

This study was supported by the National Science and Technology Council (NSTC) of Taiwan, jointly both grant numbers of NSTC 112-2221-E-992-015 from the National Science and Technology Council and of K11138 from National Kaohsiung University of Science and Technology, Taiwan, R.O.C. Acknowledgements also go to the NCEP for providing the GFS data that drove the WRF forecasts, to the CWA for the meteorological data, and to the EPA for the air quality data.

CONFLICT OF INTEREST

The authors declare no conflict of interest.

REFERENCES

Ali, Z., Shahzadi, K., Sidra, S., Zona, Z., Zainab, I., Aziz, K., Ahmad, M., Raza, S.T., Nasir, Z.A., Colbeck, I. (2015). Seasonal variation of particulate matter in the ambient conditions of Khanspur, Pakistan. J. Anim. Plant Sci. 25, 700–705. https://www.thejaps.org.pk/docs/Supplementary/v-25-sup-2/65.pdf

Alizadeh Choobari, O., Zawar-Reza, P., Sturman, A. (2012). Feedback between windblown dust and planetary boundary-layer characteristics: Sensitivity to boundary and surface layer

parameterizations. Atmos. Environ. 61, 294–304. https://doi.org/10.1016/j.atmosenv.2012.07.038

Alizadeh-Choobari, O., Bidokhti, A.A., Ghafarian, P., Najafi, M.S. (2016). Temporal and spatial variations of particulate matter and gaseous pollutants in the urban area of Tehran. Atmos. Environ. 141, 443–453. https://doi.org/10.1016/j.atmosenv.2016.07.003

Amodio, M., Andriani, E., Angiuli, L., Assennato, G., de Gennaro, G., Di Gilio, A., Giua, R., Intini, M., Menegotto, M., Nocioni, A., Palmisani, J., Perrone, M.R., Placentino, C.M., Tutino, M. (2011). Chemical characterization of PM in the Apulia Region: local and long-range transport contributions to particulate matter. Boreal Environ. Res. 16, 251–261. https://www.borenv.net/BER/archive/pdfs/ber16/ber16-251.pdf

Birman, V.K., Meiburg, E., Ungarish, M. (2007). On gravity currents in stratified ambients. Phys. Fluids 19, 086602. https://doi.org/10.1063/1.2756553

Boadh, R., Satyanarayana, A.N.V., Rama Krishna, T.V.B.P.S., Madala, S. (2016). Sensitivity of PBL schemes of the WRF-ARW model in simulating the boundary layer flow parameters for their application to air pollution dispersion modeling over a tropical station. Atmósfera https://doi.org/10.20937/ATM.2016.29.01.05

Chan, K. (2017). Aerosol optical depths and their contributing sources in Taiwan. Atmos. Environ. 148, 364–375. https://doi.org/10.1016/j.atmosenv.2016.11.011

Chen, F.C., Kuo, Y.H. (2006). Topographic effects on a wintertime cold front in Taiwan. Mon. Weather Rev. 134, 3297–3316. https://doi.org/10.1175/MWR3255.1

Chen, T.J., Chen, H.J. (1987). Study on large-scale features of dust storm system in East Asia. Meteorol. Res. 10, 57–79.

Chen, Y.L., Hui, N.B.F. (1990). Analysis of a shallow front during the Taiwan area mesoscale experiment. Mon. Weather Rev. 118, 2649–2667. https://doi.org/10.1175/1520-0493(1990)118<2649:AOASFD>2.0.CO;2

Chuang, Y.H., Chen, H.W., Chen, W.Y., Teng, Y.C. (2016). Establishing Mechanism of Warning for River Dust Event Based on an Artificial Neural Network, in: Hirose, A., Ozawa, S., Doya, K., Ikeda, K., Lee, M., Liu, D. (Eds.), Neural Information Processing, Springer International Publishing, Cham, pp. 51–60. https://doi.org/10.1007/978-3-319-46687-3_6

Crouvi, O., Dayan, U., Amit, R., Enzel, Y. (2017). An Israeli haboob: Sea breeze activating local anthropogenic dust sources in the Negev loess. Aeolian Res. 24, 39–52. https://doi.org/10.1016/j.aeolia.2016.12.002

Duce, R.A., Unni, C.K., Ray, B.J., Prospero, J.M., Merrill, J.T. (1980). Long-range atmospheric transport of soil dust from Asia to the tropical North Pacific: Temporal variability. Science 209, 1522–1524. https://doi.org/10.1126/science.209.4464.1522

Dudhia, J. (1989). Numerical study of convection observed during the winter monsoon experiment using a mesoscale two dimensional model. J. Atmos. Sci. 46, 3077–3107. https://doi.org/10.1175/1520-0469(1989)046<3077:NSOCOD>2.0.CO;2

Dudhia, J. (1996). A multi-Layer soil temperature model for MM5 Sixth Annual PSU/NCAR Mesoscale Model Users' Workshop, Bouilder, CO, 22-24 July 1996, pp. 49–50. https://www.researchgate.net/publication/259865197_A_Multi-layer_Soil_Temperature_Model_for_MM5

Evan, A.T., Porter, W., Clemesha, R., Kuwano, A., Frouin, R. (2022). Measurements of a dusty density current in the western Sonoran Desert. J. Geophys. Res.: Atmos. 127, e2021JD035830. https://doi.org/10.1029/2021JD035830

Fekih, A., Mohamed, A. (2019). Evaluation of the WRF model on simulating the vertical structure and diurnal cycle of the atmospheric boundary layer over Bordj Badji Mokhtar (southwestern Algeria). J. King Saud Univ. Sci. 31, 602–611. https://doi.org/10.1016/j.jksus.2017.12.004

Hallworth, M.A., Huppert, H.E., Ungarish, M. (2001). Axisymmetric gravity currents in a rotating system: experimental and numerical investigations. J. Fluid Mech. 447, 1–29. https://doi.org/10.1017/S0022112001005523

Hariprasad, K.B.R.R., Srinivas, C.V., Bagavath Singh, A., Vijaya, Bhaskara Rao S., Baskaran, R., Venkatraman, B. (2014). Numerical simulation and intercomparison of boundary layer structure with different PBL schemes in WRF using experimental observations at a tropical site. Atmos. Res. 145, 27–44. https://doi.org/10.1016/j.atmosres.2014.03.023

Hong, J.S., Lin, D.E., Chien, F.C., Liu, S.P., Jou, Ben J.D., Lin, P.L., Chang, W.J. Miou, H.J. Chen, C.Y.,

Lei, M.C. (2006). A sensitivity study of the WRF Model Part I: Verification over radiosound observation. Atmos. Sci. 34, 241–260. (in Chinese with English abstract)

Hong, S.Y., Dudhia, J., Chen, S.H. (2004). A revised approach to ice microphysical processes for the bulk parameterization of clouds and precipitation. Mon. Weather Rev. 132, 103–120. https://doi.org/10.1175/1520-0493(2004)132<0103:ARATIM>2.0.CO;2

Hong, S.Y. (2010). A new stable boundary-layer mixing scheme and its impact on the simulated East Asia summer monsoon. Q. J. R. Meteorol. Soc. 136, 1481–1496. https://doi.org/10.1002/qj.665

Houze, R.A.J. (1993). Cloud Dynamics. Academic Press, San Diego.

Hsieh, M.K., Chen, Y.W., Chen, Y.C., Wu, C.M. (2022). The roles of local circulation and boundary layer development in tracer transport over complex topography in central Taiwan. J. Meteorol. Soc. Jpn. 100, 555–573. https://doi.org/10.2151/jmsj.2022-028

Hsu, C.H., Cheng, F.Y. (2016). Classification of weather patterns to study the influence of meteorological characteristics on $PM_{2.5}$ concentrations in Yunlin County, Taiwan. Atmos. Environ. 144, 397–408. https://doi.org/10.1016/j.atmosenv.2016.09.001

Hsu, C.H., Cheng, F.Y. (2019). Synoptic weather patterns and associated air pollution in Taiwan. Aerosol Air Qual. Res. 19, 1139–1151. https://doi.org/10.4209/aaqr.2018.09.0348

Hsu, C.Y., Lin, M.Y., Chiang, H.C., Chen, M.J., Lin, T.Y., Chen, Y.C. (2016). Using a mobile measurement to characterize number, surface area, and mass concentrations of ambient fine particles with spatial variability during and after a PM event. Aerosol Air Qual. Res. 16, 1416–1426. https://doi.org/10.4209/aaqr.2014.12.0311

Huang, X., Wang, Z., Ding, A. (2018). Impact of aerosol-PBL Interaction on haze pollution: multiyear observational evidences in North China. Geophys. Res. Lett. 45, 8596–8603. https://doi.org/10.1029/2018GL079239

Hung, C.H., Lo, K.C. (2015). Relationships between ambient ozone concentration changes in Southwestern Taiwan and invasion tracks of tropical typhoons. Adv. Meteorol. 2015, 402976. https://doi.org/10.1155/2015/402976

Hung, C.H., Lo, K.C., Yuan, C.S. (2018). Forming highly polluted PMs caused by the invasion of transboundary air pollutants: Model simulation and discussion. Aerosol Air Qual. Res. 18, 1698–1719. https://doi.org/10.4209/aaqr.2017.11.0488

Huppert, H.E. (1982). The propagation of two-dimensional and axisymmetric viscous gravity currents over a rigid horizontal surface. J. Fluid Mech. 121, 43–58. https://doi.org/10.1017/S0022112082001797

Ising, J., Kaplan, M.L., Lin, Y.L. (2022). Effects of density current, diurnal heating, and local terrain on the mesoscale environment conducive to the Yarnell Hill Fire. Atmosphere 13, 215. https://doi.org/10.3390/atmos13020215

Kain, J.S., Fritsch, J.M. (1993). Convective Parameterization for Mesoscale Models: The Kain-Fritsch Scheme, in: Emanuel, K.A., Raymond, D.J. (Eds.), The Representation of Cumulus Convection in Numerical Models, American Meteorological Society, Boston, MA, pp. 165–170. https://doi.org/10.1007/978-1-935704-13-3_16

Kartsios, S., Pytharoulis, I., Karacostas, T., Pavlidis, V., Katragkou, E. (2024). Verification of a global weather forecasting system for decision-making in farming over Africa. Acta Geophys. 72, 467–488. https://doi.org/10.1007/s11600-023-01136-y

Kuo, C.Y., Hsieh, C.Y., Hu, C.W., Chen, S.C., Yang, H.J. (2017). PM_{10} concentration in relation to clinic visits for anxiety disorders: a population-based study of a high river-dust event region in Taiwan. Air Qual. Atmos. Health 11, 221–227. https://doi.org/10.1007/s11869-017-0534-4

Kuo, C.Y., Lin, C.Y., Huang, L.M., Wang, S., Shieh, P.F., Lin, Y.R., Wang, J.Y. (2010). Spatial variations of the aerosols in river-dust events in Central Taiwan. J. Hazard Mater. 179, 1022–1030. https://doi.org/10.1016/j.jhazmat.2010.03.107

Kuo, C.Y., Yang, H.J., Chiang, Y.C., Lai, D.J., Shen, Y.H., Liu, P.M. (2014). Concentration and composition variations of metals in the outdoor PM_{10} of elementary schools during river dust episodes. Environ. Sci. Pollut. Res. 21, 12354–12363. https://doi.org/10.1007/s11356-014-3179-y

Lagouvardos, K., Kotroni, V., Kallos, G. (1988). An extreme cold surge over the Greek peninsula. Q. J. R. Meteorol. Soc. 124, 2299–2327. https://doi.org/10.1002/qj.49712455107

Largeron Y., Staquet, C. (2016). Persistent inversion dynamics and wintertime PM_{10} air pollution in Alpine valleys. Atmos. Environ. 135, 92–108. https://doi.org/10.1016/j.atmosenv.2016.03.045

Li, J., Yu, S., Chen, X., Zhang, Y., Li, M., Li, Z., Song, Z., Liu, W., Li, P., Xie, M., Xing, J. (2022). Evaluation of the WRF-CMAQ model performances on air quality in China with the impacts of the observation nudging on meteorology. Aerosol Air Qual. Res. 22, 220023. https://doi.org/10.4209/aaqr.220023

Li, Z., Guo, J., Ding, A., Liao, H., Liu, J., Sun, Y., Wang, T., Xue, H., Zhang, H., Zhu, B. (2017). Aerosol and boundary-layer interactions and impact on air quality. Natl. Sci. Rev. 4, 810–833. https://doi.org/10.1093/nsr/nwx117

Lin, C., Liu, S., Chou, C., Huang, S., Liu, C., Kuo, C., Young, C. (2005). Long-range transport of aerosols and their impact on the air quality of Taiwan. Atmos. Environ. 39, 6066–6076. https://doi.org/10.1016/j.atmosenv.2005.06.046

Lin, C.Y., Liu, S.C., Chou, C.C.K., Liu, T.H., Lee, C.T., Yuan, C.S., Shiu, C.J., Young, C.Y. (2004). Long-range transport of Asian dust and air pollutants to Taiwan. Terr. Atmos. Ocean. Sci. 15, 759–784. https://doi.org/10.3319/TAO.2004.15.5.759(ADSE)

Lin, C.Y., Wang, Z., Chen, W.N., Chang, S.Y., Chou, C.C.K., Sugimoto, N., Zhao, X. (2007). Long-range transport of Asian dust and air pollutants to Taiwan: observed evidence and model simulation. Atmos. Chem. Phys. 7, 423–434. https://doi.org/10.5194/acp-7-423-2007

Lin, C.Y., Sheng, Y.F., Chen, W.N., Wang, Z., Kuo, C.H., Chen, W.C., Yang, T. (2012). The impact of channel effect on Asian dust transport dynamics: a case in southeastern Asia. Atmos. Chem. Phys. 12, 271–285. https://doi.org/10.5194/acp-12-271-2012

Lin, C.Y., Chiang, M.L., Lin, C.Y. (2016). Empirical model for evaluating PM_{10} concentration caused by river dust events. Int. J. Environ. Res. Publ. Health 13, 553. https://doi.org/10.3390/ijerph13060553

Lin, C.Y., Lee, Y.H., Kuo, C.Y., Chen, W.C., Sheng, Y.F., Su, C.J. (2018). Impact of river-dust events on air quality of western Taiwan during winter monsoon: Observed evidence and model simulation. Atmos. Environ. 192, 160–172. https://doi.org/10.1016/j.atmosenv.2018.08.048

Lin, T.H. (2001). Long-range transport of yellow sand to Taiwan in spring 2000: Observed evidence and simulation. Atmos. Environ. 35, 5873–5882. https://doi.org/10.1016/S1352-2310(01)00392-2

Madala, S., Salyanarayana, A.N.V., Srinivas, C.V., Kumar, M. (2015). Mesoscale atmospheric flow-field simulations for air quality modeling over Complex terrain region of Ranchi in Eastern India using WRF. Atmos. Environ. 107, 315–328. https://doi.org/10.1016/j.atmosenv.2015.02.059

Mlawer, E.J., Taubman, S.J., Brown, P.D., Iacono, M.J., Clough, S.A. (1997). Radiative transfer for inhomogeneous atmospheres: RRTM, a validated correlated-k model for the longwave. J. Geophys. Res. 102, 16663–16682. https://doi.org/10.1029/97JD00237

Mobarak Hassan, E., Alizadeh, O. (2022). Dust events in southwestern Iran: Estimation of PM_{10} concentration based on horizontal visibility during dust events. Int. J. Climatol. 42, 5159–5172. https://doi.org/10.1002/joc.7525

Musumeci, R.E., Viviano, A., Foti, E. (2017). Influence of regular surface waves on the propagation of gravity currents: Experimental and numerical modelling. J. Hydraul. Eng. 143, 04017022. https://doi.org/10.1061/(ASCE)HY.1943-7900.0001308

Olofson, K., Andersson, P., Hallquist, M., Ljungstr€om, E., Tang, L., Chen, D., Pettersson, J. (2009). Urban aerosol evolution and particle formation during wintertime temperature inversions. Atmos. Environ. 43, 340–346. https://doi.org/10.1016/j.atmosenv.2008.09.080

Park, S.U., Park, M.S., Chun, Y. (2010). Asian dust events observed by a 20-m monitoring tower in Mongolia during 2009. Atmos. Environ. 44, 4964–4972. https://doi.org/10.1016/j.atmosenv.2010.08.014

Parrington, J.R., Zoller, W.H., Aras, N.K. (1983). Asian dust: Seasonal transport to the Hawaiian Islands. Science 220, 195–197. https://doi.org/10.1126/science.220.4593.195

Prospero, J.M., Savoie, D.L., Arimoto, R. (2003). Long-term record of nss-sulfate and nitrate in aerosols on Midway Island, 1981–2000: Evidence of increased (now decreasing?) anthropogenic emissions from Asia. J. Geophys. Res. 108, 4019. https://doi.org/10.1029/2001JD001524

Sabetghadam, S., Alizadeh, O., Khoshsima, M., Pierleoni, A. (2021). Aerosol properties, trends

and classification of key types over the Middle East from satellite-derived atmospheric optical data. Atmos. Environ. 246, 118100. https://doi.org/10.1016/j.atmosenv.2020.118100

Sabetghadam, S., Khoshsima, M., Alizadeh-Choobari, O. (2018). Spatial and temporal variations of satellite-based aerosol optical depth over Iran in Southwest Asia: Identification of a regional aerosol hot spot. Atmos. Pollut. Res. 9, 849–856. https://doi.org/10.1016/j.apr.2018.01.013

Shaw, G.E. (1980). Transport of Asian desert aerosol to Hawaiian Islands. J. Appl. Meteorol. 19, 1254–1259. https://doi.org/10.1175/1520-0450(1980)019<1254:TOADAT>2.0.CO;2

Silva, P., Vawdrey, E., Corbett, M., Erupe, M. (2007). Fine particle concentrations and composition during wintertime inversions in Logan, Utah, USA. Atmos. Environ. 41, 5410–5422. https://doi.org/10.1016/j.atmosenv.2007.02.016

Smith, R. K., Reeder, M.J. (1988). On the movement and low-level structure of cold fronts. Mon. Weather Rev. 116, 10, 1927–1044. https://doi.org/10.1175/1520-0493(1988)116<1927:OTMALL>2.0.CO;2

Soleimanpour, M., Alizadeh, O., Sabetghadam, S. (2023). Analysis of diurnal to seasonal variations and trends in air pollution potential in an urban area. Sci. Rep. 13, 21065. https://doi.org/10.1038/s41598-023-48420-x

Souza, N.B.P., Nascimento, E.G.S., Moreira, D.M. (2023). Performance evaluation of the WRF model in a tropical region: Wind speed analysis at different sites. Atmósfera 36, 253–277. https://doi.org/10.20937/ATM.52968

Stancanelli, L.M., Musumeci, R.E., Foti, E. (2018). Dynamics of gravity currents in the presence of surface waves. J. Geophys. Res.: Oceans 123, 2254–2273. https://doi.org/10.1002/2017JC013273

Sun, Z., Zhang, X., Zhao, X., Xia, X., Miao, S., Li, Z., Cheng, Z., Wen, W., Tang, Y. (2018). Oscillation of surface $PM_{2.5}$ concentration resulting from an alternation of easterly and southerly winds in Beijing: Mechanisms and implications. J. Meteorol. Res. 32, 288–301. https://doi.org/10.1007/s13351-018-7064-3

Sun, Z., Wang, H., Guo, C., Wu, J., Cheng, T., Li, Z. (2019). Barrier effect of terrain on cold air and return flow of dust air masses. Atmos. Res. 220, 81–91. https://doi.org/10.1016/j.atmosres.2019.01.007

Sun, Z., Zhao, X., Li, Z., Tang, G., Miao, S. (2021). Boundary layer structure characteristics under objective classification of persistent pollution weather types in the Beijing area. Atmos. Chem. Phys. 21, 8863–8882. https://doi.org/10.5194/acp-21-8863-2021

Tsai, D.M., Lai, H.C., Zhang, H.L., Yang, R.Y., Chiou, H.C. (2020). Establishment of real-time three-dimensional meteorological and air quality forecasting system for ship emission. Research projects, Institute of Transportation, Ministry of Transportation and Communications. pp. 257. (in Chinese with English abstract)

Wallace, J., Kanaroglou, P. (2009). The effect of temperature inversions on ground-level nitrogen dioxide (NO_2) and fine particulate matter ($PM_{2.5}$) using temperature profiles from the Atmospheric Infrared Sounder (AIRS). Sci. Total Environ. 407, 5085–5095. https://doi.org/10.1016/j.scitotenv.2009.05.050

Wang, L., Liu, Z., Sun, Y., Ji, D., Wang, Y. (2015). Long-range transport and regional sources of $PM_{2.5}$ in Beijing based on long-term observations from 2005 to 2010. Atmos. Res. 157, 37–48. https://doi.org/10.1016/j.atmosres.2014.12.003

Wang, W.C., Chen, K.S. (2008). Modeling and analysis of source contribution of PM_{10} during severe pollution events in Southern Taiwan. Aerosol Air Qual. Res. 8, 319–338. https://doi.org/10.4209/aaqr.2008.06.0020

Wang, Z., Itahashi, S., Uno, I., Pan, X., Osada, K., Yamamoto, S., Nishizawa, T., Tamura, K., Wang, Z. (2017). Modeling the long-range transport of particulate matters for January in East Asia using NAQPMS and CMAQ. Aerosol Air Qual. Res. 17, 3064–3078. https://doi.org/10.4209/aaqr.2016.12.0534

Wang, Z., Ueda, H., Huang, M. (2000). A deflation module for use in modeling long-range transport of yellow sand over East Asia. J. Geophys. Res. 105, 26947–26959. https://doi.org/10.1029/2000JD900370

Weng, T.H., Lee, Y.C., Chen, W.H., Lin, Y.S., Su, Y.C., Tong, Y.H., Chang, J.S., Tsai, Y.I. (2021). Verification of fugitive emission of aeolian river dust and impact on air quality in central

western Taiwan by observed evidence and simulation. Atmos. Pollut. Res. 12, 101139. https://doi.org/10.1016/j.apr.2021.101139

Wuebbles, D.J., Lei, H., Lin, J.T. (2007). Intercontinental transport of aerosols and photochemical oxidants from Asia and its consequences. Environ. Pollut. 150, 65–84. https://doi.org/10.1016/j.envpol.2007.06.066

Xing, Q., Sun, M. (2022). Characteristics of $PM_{2.5}$ and PM_{10} spatial-temporal distribution and influencing meteorological conditions in Beijing. Atmosphere 13, 1120. https://doi.org/10.3390/atmos13071120

Xu, Y., Zhu, B., Shi, S.H. (2019). Two inversion layers and their impacts on $PM_{2.5}$ concentration over the Yangtze River Delta, China. J. Appl. Meteorol. Climatol. 58, 2349–2362. https://doi.org/10.1175/JAMC-D-19-0008.1

Zhai, L., Sun, Z., Li, Z., Yin, X., Xiong, Y., Wu, J., Li, E., Kou, X. (2019). Dynamic effects of topography on dust particles in the Beijing region of China. Atmos. Environ. 213, 413–423. https://doi.org/10.1016/j.atmosenv.2019.06.029

Zhang, B., Jiao, L., Xu, G., Zhao, S., Tang, X., Zhou, Y., Gong, C. (2018). Influences of wind and precipitation on different-sized particulate matter concentrations ($PM_{2.5}$, PM_{10}, $PM_{2.5–10}$). Meteorol. Atmos. Phys. 130, 383–392. https://doi.org/10.1007/s00703-017-0526-9

Zhang, L., Cheng, Y., Zhang, Y., He, Y., Gu, Z., Yu, C. (2017). Impact of air humidity fluctuation on the rise of PM mass concentration based on the high-resolution monitoring data. Aerosol Air Qual. Res. 17, 543–552. https://doi.org/10.4209/aaqr.2016.07.0296

Zhang, Y.H., Zhang, S.D., Yi, F. (2009). Intensive radiosonde observations of lower tropospheric inversion layers over Yichang, China. J. Atmos. Sol. Terr. Phys. 71, 180–190. https://doi.org/10.1016/j.jastp.2008.10.008